



1 Downpour Dynamics: Outsized impacts of storm events 2 on unprocessed atmospheric nitrate export in an urban 3 watershed

4 Joel T. Bostic^{1,2}, David M. Nelson¹, Keith N. Eshleman¹

5 ¹University of Maryland Center for Environmental Science, Appalachian Lab, Frostburg, Maryland,
6 USA

7 ²Potomac State College of West Virginia University, Keyser, West Virginia, USA

8 *Correspondence to:* Joel Bostic (joel.bostic@mail.wvu.edu)

9 **Abstract.** Water-quality impacts of streamwater nitrate (NO_3^-) on downstream ecosystems are largely
10 determined by the load of NO_3^- from the watershed to surface waters. The largest NO_3^- loads often
11 occur during storm events, but it is unclear how loads of different NO_3^- sources change during storm
12 events relative to baseflow or how watershed attributes might affect source export. To assess the role
13 of stormflow and baseflow on NO_3^- source export and how these roles are modulated by hydrologic
14 effects of land-use practices, we measured nitrogen ($\delta^{15}\text{N}$) and triple oxygen ($\Delta^{17}\text{O}$) isotopes of NO_3^-
15 and oxygen isotopes ($\delta^{18}\text{O}$) of water in rainfall and streamwater samples from before, during, and after
16 8 storm events across 14 months in two Chesapeake Bay watersheds of contrasting land-use. Storms
17 had a disproportionately large influence on the export of unprocessed atmospheric NO_3^- ($\text{NO}_3^-_{\text{Atm}}$) and
18 a disproportionately small influence on export of terrestrial NO_3^- ($\text{NO}_3^-_{\text{Terr}}$) relative to baseflow in the
19 developed urban watershed. In contrast, baseflow and stormflow had similar influences on $\text{NO}_3^-_{\text{Atm}}$
20 and $\text{NO}_3^-_{\text{Terr}}$ export in the mixed agricultural/forested watershed. An equivalent relationship between
21 $\text{NO}_3^-_{\text{Atm}}$ deposition on impervious surfaces and event $\text{NO}_3^-_{\text{Atm}}$ streamwater export in the urban
22 watershed suggests that impervious surfaces that hydrologically connect runoff to channels likely
23 facilitate export of $\text{NO}_3^-_{\text{Atm}}$ during rainfall events. Additionally, larger rainfall events were more
24 effective in exporting $\text{NO}_3^-_{\text{Atm}}$ in the urban watershed, with increased rainfall depth resulting in a
25 greater fraction of event $\text{NO}_3^-_{\text{Atm}}$ deposition exported. Considering both projected increases in
26 precipitation amounts and intensity and urban/suburban sprawl in many regions of the world, best
27 management practices that reduce hydrologic connectivity of impervious surfaces will likely help to
28 mitigate the impact of storm events on $\text{NO}_3^-_{\text{Atm}}$ export from developed watersheds.



29

30 **1 Introduction**

31 Increasing streamwater nitrate (NO_3^-) export over the past century has negatively impacted
32 many downstream ecosystems globally (Kemp et al., 2005; Camargo and Alonso, 2006; Steffen et al.,
33 2015; Stevens, 2019). The severity of impacts to receiving waters is partially determined by the
34 magnitude of NO_3^- loads (i.e., product of concentration and discharge; NRC, 2000). As such, riverine
35 NO_3^- loads are greatest during periods of high discharge, which often follow large precipitation
36 events, and can therefore have an outsized impact on annual streamwater NO_3^- loads (Vaughan et al.,
37 2017; Kincaid et al., 2020). Sources of NO_3^- comprising storm event loads can be variable and
38 associated with changing hydrologic flowpaths during precipitation events (Buda and DeWalle, 2009).
39 Loads of individual NO_3^- sources (e.g., atmospheric NO_3^-) exported during storm events are rarely
40 quantified, however (Divers et al., 2014; Sabo et al., 2016). Thus, it is not clear whether storm events
41 have a disproportionate impact relative to non-storm (i.e., baseflow) conditions on different NO_3^-
42 sources. The impact of storm events relative to baseflow on sources of streamwater NO_3^- is
43 particularly relevant given the increases in precipitation amount and intensity projected to be
44 associated with future climate change (Walsh et al., 2014).

45 Precipitation can affect the amount, as well as the source, of NO_3^- exported in surface waters
46 via the surface-to-stream flow path. During storms, NO_3^- can be transported to streams by either
47 overland or subsurface pathways. Overland flow is associated with NO_3^- sources deposited or present
48 on the land surface, such as unprocessed atmospheric NO_3^- ($\text{NO}_3^-_{\text{Atm}}$; Rose et al., 2015a). Subsurface
49 flow is associated with NO_3^- sources abundant in soils and groundwater, such as fertilizer, microbial,
50 and/or sewage (Cook and Herczeg, 2012). Both hydrologic flowpaths (and the respective NO_3^-
51 sources) can be affected by human land-use activities (Paul and Meyer, 2001; Barnes and Raymond,
52 2010; Jarvis, 2020). For example, previous studies report that developed watersheds export relatively
53 more $\text{NO}_3^-_{\text{Atm}}$ than less developed watersheds, presumably due to hydrologic changes created by
54 impervious surfaces (Buda and DeWalle, 2009; Burns et al., 2009; Kaushal et al., 2011; Bostic et al.,
55 2021). However, evidence is lacking for (1) the mechanism generating increased $\text{NO}_3^-_{\text{Atm}}$ export in



56 developed watersheds and (2) quantitative impacts of storm event loads relative to baseflow, both of
57 which could be useful for mitigating the effects of storms on streamwater NO_3^- export.

58 The stable isotope compositions of NO_3^- and water (H_2O) are powerful tools for
59 distinguishing NO_3^- sources and hydrologic flow paths, respectively. For example, the triple oxygen
60 isotope values ($\Delta^{17}\text{O}$) of NO_3^- allow for quantification of atmospheric and terrestrial sources of NO_3^-
61 in streamwater (Michalski et al., 2003), and $\delta^{15}\text{N}$ and $\delta^{18}\text{O}$ values of NO_3^- permit inferences into the
62 relative contributions of terrestrially-sourced NO_3^- ($\text{NO}_3^-_{\text{Terr}}$), such as fertilizer or sewage N (Kendall
63 et al., 2007). Additionally, $\delta^{18}\text{O}$ values of H_2O can be used to assess the importance of overland versus
64 subsurface flow through partitioning of stream flow into pre-event and event contributions (Sklash et
65 al., 1976; McGuire and McDonnell, 2007). Few studies have coupled these isotopic tracers (Buda and
66 DeWalle, 2009), however, despite their suitability to assess the effect of storm events on both
67 hydrologic flow paths and export of different NO_3^- sources. Such information could provide
68 mechanistic evidence for the commonly reported relationship between developed watersheds and
69 $\text{NO}_3^-_{\text{Atm}}$ export.

70 Here we address the following research questions: How do storm events affect the total
71 amount and sources of NO_3^- exported in streams relative to baseflow? And, more specifically, what is
72 the relationship between hydrologic and biogeochemical effects of land use and the export of
73 unprocessed atmospheric $\text{NO}_3^-_{\text{Atm}}$ and terrestrial NO_3^- during storm events and baseflow? These
74 questions were addressed in two Chesapeake Bay watersheds of contrasting land-use. A two-watershed
75 study is inherently comparative, potentially limiting the inferences that can be made regarding land-use
76 effects. However, given the contrasting land uses (i.e., predominantly developed compared to mixed
77 forest/agriculture) in these watersheds, we believe that this study can adequately address our research
78 questions while presenting a “proof of concept” for future studies. To address these research questions,
79 we collected moderate-frequency streamwater samples before, during, and after eight rainfall events,
80 bulk rainfall samples corresponding to these events, as well as monthly baseflow samples, in two
81 catchments within the broader Chesapeake Bay watershed. We then used $\delta^{15}\text{N}$, $\delta^{18}\text{O}$, and $\Delta^{17}\text{O}$ of
82 NO_3^- and $\delta^{18}\text{O}$ of H_2O to determine NO_3^- sources and hydrologic flowpaths, respectively. The
83 Chesapeake Bay region is ideal for our study: it is one of the most ecologically and economically



84 important estuaries in the world (NOAA, 1990) that has experienced recent improvements in
85 ecosystem health associated with declining N loads (Chanat et al., 2016; Lefcheck et al., 2018; Zhang
86 et al., 2018), but uncertainty surrounds continued water quality improvements in part due to the effects
87 of projected increases in precipitation intensity across its diverse land-use watershed (Najjar et al.,
88 2010).

89 **2 Materials and Methods**

90 **2.1 Study watersheds and field methods**

91 To assess NO_3^- export dynamics during storm events, streamwater and rainfall samples were
92 collected synchronously during eight events from two watersheds with outlets in Maryland, USA –
93 Gwynns Falls at Villa Nova (GWN) and Gunpowder Falls at Glencoe (GUN) (Figure 1) – from
94 September 2018 – October 2019. These watersheds have similar geology (Piedmont physiographic
95 province; Fenneman, 1946) and climate (humid sub-tropical; Kottek et al., 2006), but differing land-
96 use (one predominantly developed and the other mixed forest and agriculture), impervious surface
97 coverage (Figure S1) and area (Table 1). Events were targeted based on forecast precipitation amounts
98 of at least 2.5 cm and the same events were sampled at each site. Automated samplers (Teledyne ISCO
99 3700 Portable Sampler, Lincoln, NE) were used to collect streamwater samples into pre-cleaned 1L
100 bottles across each storm hydrograph, including pre-storm baseflow, rising limbs, and falling limbs for
101 most events at intervals ranging from 45 minutes – 12 hours (Figure S2). Storm sample collection
102 ceased when discharge fell to approximately 200% of pre-event baseflow. Bulk rainfall samples
103 corresponding to each event were collected using 7.5 cm diameter funnels approximately 1 m above
104 ground level connected to pre-cleaned 1 L Nalgene bottles, with pre-cleaned table tennis balls used to
105 limit evaporation. Streamwater and rainfall samples were placed on ice for 12 – 36 hours after
106 collection, then processed in the laboratory within 24 – 48 hours. Both study watersheds are gaged by
107 the United States Geological Survey; 15-minute and mean daily discharge data were obtained using the
108 dataRetrieval R package (DeCicco, 2018). Mean event rainfall depth for each watershed was obtained
109 from PRISM Climate Group (PRISM, 2014) using the prism R package (Hart and Bell, 2015).



110 2.2 Lab Methods

111 Streamwater and rainfall samples for NO_3^- concentration and isotope analyses were filtered (0.45 μm)
112 and frozen within 48 hours of collection. Aliquots for water isotope measurements were stored in
113 completely filled (i.e., no headspace) 20 mL bottles at room temperature prior to analysis. NO_3^- and
114 nitrite (NO_2^-) concentrations were measured using flow-injection colorimetric analysis (Lachat
115 Quikchem 8000 FIA+).

116 The $\Delta^{17}\text{O}$, $\delta^{18}\text{O}$, and $\delta^{15}\text{N}$ values of stream and rainfall NO_3^- were measured using a Thermo
117 Delta V+ isotope ratio mass spectrometer (Bremen, Germany) via the denitrifier method (Sigman et
118 al., 2001; Casciotti et al., 2002) with thermal decomposition (at 800° C) of N_2O to N_2 and O_2 (Kaiser et
119 al., 2007) at the Central Appalachians Stable Isotope Facility. NO_2^- is denitrified using this method as
120 well, but NO_2^- concentrations in stream and rainfall samples were low relative to NO_3^- ($\text{NO}_2^-/(\text{NO}_2^- +$
121 $\text{NO}_3^-)$ mean = 0.006, range = 0.00 – 0.027). Measured isotope ratios were normalized using
122 international reference standards USGS 34 ($\delta^{17}\text{O} = -14.8$ ‰, $\delta^{18}\text{O} = -27.9$ ‰) and USGS 35 ($\delta^{17}\text{O} =$
123 51.5 ‰, $\delta^{18}\text{O} = 57.5$ ‰) for O isotopes (Böhlke et al., 2003) and USGS 32 ($\delta^{15}\text{N} = 180$ ‰) and USGS
124 34 ($\delta^{15}\text{N} = -1.8$ ‰) for N isotopes (IAEA, 1995). Reference standards were measured throughout
125 sample analysis in equal concentrations to samples (ranging from 100 – 200 nmol depending on
126 sample NO_3^- concentration). Analytical precision of $\Delta^{17}\text{O}$ ($\Delta^{17}\text{O} \approx \delta^{17}\text{O} - 0.52 \times \delta^{18}\text{O}$) was estimated
127 as 0.5 ‰, $\delta^{18}\text{O}$ as 1.4 ‰, and $\delta^{15}\text{N}$ as 1.8 ‰ (1 σ), based on repeated measurements ($n \approx 200$) of
128 reference standards USGS 32 and USGS 35 and a laboratory reference standard “Chile NO_3^- ” (Duda
129 Energy 1sn 1 lb. Sodium Nitrate Fertilizer 99+% Pure Chile Saltpeter from Amazon.com). Accuracy of
130 $\Delta^{17}\text{O}$, $\delta^{18}\text{O}$, and $\delta^{15}\text{N}$ were tracked using repeated measurements of IAEA-N3 ($n = 19$, mean $\Delta^{17}\text{O} = -$
131 0.1 ‰, $\delta^{18}\text{O} = 24.3$ ‰, $\delta^{15}\text{N} = 4.5$ ‰) and closely agreed with published values (IAEA, 1995;
132 Michalski et al., 2002; Böhlke et al., 2003). Each streamwater and rainfall sample was measured 3 – 6
133 times to reduce analytical uncertainty and the mean of each sample was used in all analyses. Standard
134 error of the mean ranged from 0.1 – 0.6 ‰, 0.1 – 1.6 ‰, and 0.1 – 1.6 ‰ for replicate measurements
135 of $\Delta^{17}\text{O}$, $\delta^{18}\text{O}$, and $\delta^{15}\text{N}$ respectively.



136 Oxygen ($\delta^{18}\text{O}_{\text{H}_2\text{O}}$) isotopes of rainfall and streamwater were measured using a Picarro L2130-
137 i via cavity ring down spectroscopy at the University of Wyoming Stable Isotope Facility. Measured
138 isotope ratios were normalized to VSMOW using internal laboratory standards that were calibrated to
139 international standards. Precision based on repeated measurements of internal standards was 0.2 %.

140 2.3 Quantification of atmospheric NO_3^- deposition

141 Event $\text{NO}_3^-_{\text{Atm}}$ deposition was quantified using the measured rainfall NO_3^- concentration and
142 mean rainfall depth:

$$143 \text{NO}_3^-_{\text{Atm}} \text{Deposition (g N ha}^{-1}\text{)} = \frac{\text{Rainfall Volume (L)} \times \text{Rainfall NO}_3^- \text{(mg N L}^{-1}\text{)}}{\text{Watershed Area (ha)}} \times (1 \times 10^{-3}) \text{ (eq.}$$

144 1)

145 where rainfall volume is the product of rainfall depth and watershed area and 1×10^{-3} is a conversion
146 factor. Event $\text{NO}_3^-_{\text{Atm}}$ deposition onto impervious surfaces was then calculated by multiplying $\text{NO}_3^-_{\text{Atm}}$
147 deposition by the percent of impervious surfaces.

148 2.4 Quantification of unprocessed atmospheric and terrestrial NO_3^- in streams

149 Concentrations of $\text{NO}_3^-_{\text{Atm}}$ were quantified using $\Delta^{17}\text{O}$ values of terrestrial and rainfall end-
150 members and total NO_3^- concentrations:

$$151 f_{\text{Atm}} = \frac{(\Delta^{17}\text{O}_{\text{Stream}} - \Delta^{17}\text{O}_{\text{Terr}})}{(\Delta^{17}\text{O}_{\text{Precip}} - \Delta^{17}\text{O}_{\text{Terr}})} \quad \text{(eq. 2)}$$

$$152 \text{NO}_3^-_{\text{Atm}} \text{(mg N L}^{-1}\text{)} = f_{\text{Atm}} \times \text{NO}_3^-_{\text{Total}} \text{(mg N L}^{-1}\text{)} \quad \text{(eq. 3)}$$

$$153 \text{NO}_3^-_{\text{Terr}} \text{(mg N L}^{-1}\text{)} = \text{NO}_3^-_{\text{Total}} \text{(mg N L}^{-1}\text{)} - \text{NO}_3^-_{\text{Atm}} \text{(mg N L}^{-1}\text{)} \quad \text{(eq. 4)}$$

154 where $\Delta^{17}\text{O}_{\text{Stream}} = \Delta^{17}\text{O}$ of streamwater samples during either baseflow or storm events, $\Delta^{17}\text{O}_{\text{Precip}} =$
155 $\Delta^{17}\text{O}$ of rainfall for a given event, $\Delta^{17}\text{O}_{\text{Terr}} = \Delta^{17}\text{O}$ of terrestrially sourced NO_3^- which is $\cong 0 \text{ ‰}$,
156 $\text{NO}_3^-_{\text{Terr}} =$ terrestrial NO_3^- , and $\text{NO}_3^-_{\text{Total}} =$ measured streamwater NO_3^- concentrations. Uncertainty
157 in $\text{NO}_3^-_{\text{Atm}}$ was estimated by propagating analytical uncertainty from repeated measures of $\Delta^{17}\text{O}_{\text{Stream}}$
158 and $\Delta^{17}\text{O}_{\text{Precip}}$.

159 2.5 Quantification of event loads and mean concentrations and monthly loads

160 Event loads of $\text{NO}_3^-_{\text{Total}}$ and $\text{NO}_3^-_{\text{Atm}}$ were calculated as:



$$L_{NO_3^-} = \sum_{i=1}^n C_i \times V_i \times (1 \times 10^{-3}) \quad (\text{eq. 5})$$

161 where L = load of either NO_3^- Total, NO_3^- Atm, or NO_3^- Terr in g per event, C_i = concentration of either
162 NO_3^- Total or NO_3^- Atm in mg N L⁻¹ for sample i , and V_i = volume of water exported corresponding to
163 sample i in L, and 1×10^{-3} is a conversion factor (mg to g). Event yields (g N ha⁻¹ event⁻¹) of NO_3^- Total,
164 NO_3^- Atm, and NO_3^- Terr were calculated by normalizing loads by watershed area. To assess potential
165 bias between our method (eq. 5) and traditionally used methods to quantify NO_3^- Atm, we used the mean
166 daily discharge multiplied by NO_3^- Atm concentrations of each individual grab sample collected during
167 a particular event. We compared these estimated loads with the “true” load (calculated using eq. 5) and
168 calculated bias as the difference between the “true” load and loads estimated using a single sample and
169 daily average discharge. Because traditional methods commonly use mean daily discharge, we only
170 investigated bias for two events that included samples collected over one full day. We also calculated
171 the event fraction of unprocessed atmospheric NO_3^- (f_{Atm}) using $\Delta^{17}O$ (eq. 2) and $\delta^{18}O$ (substituting
172 $\delta^{18}O$ for $\Delta^{17}O$ in eq. 2 and assuming that baseflow samples for a corresponding storm represent the
173 terrestrial NO_3^- end-member $\delta^{18}O$ value).

174
175 Event mean concentrations (EMC) of NO_3^- Total and NO_3^- Atm and event mean values (EMV)
176 of $\Delta^{17}O$, $\delta^{18}O$, and $\delta^{15}N$ were calculated as:

$$EMC, EMV = \frac{\sum_{i=1}^n (C_i \times V_i)}{\sum_{i=1}^n V_i} \quad (\text{eq. 6})$$

177 where EMC = event mean concentration in mg N L⁻¹ (for NO_3^- Total and NO_3^- Atm), EMV = event mean
178 value in ‰ ($\Delta^{17}O$, $\delta^{18}O$, and $\delta^{15}N$), C_i = either concentration of NO_3^- Total or NO_3^- Atm (mg N L⁻¹) or
179 value of $\Delta^{17}O$, $\delta^{18}O$, or $\delta^{15}N$ (‰) corresponding to sample i , and V_i = volume of water exported
180 corresponding to sample i (L).

181
182 Monthly loads of NO_3^- Total were estimated using Weighted Regressions on Time, Discharge,
183 and Season Kalman Filter (WRTDS-K; Zhang and Hirsch, 2019). Regressions were calibrated using
184 the entire period of record for NO_3^- (excluding our storm samples) to generate coefficients
185 representing a greater range of hydroclimatological conditions than was realized in 13 months. NO_3^-
186 concentration data for the entire period of record were obtained from the Chesapeake Bay Program
187 water quality database (Chesapeake Bay Program, 2021). Our storm samples were excluded to



188 generate similar estimates of monthly and annual loads used by monitoring agencies (e.g., Maryland
189 Department of Natural Resources, US Environmental Protection Agency) in these watersheds.
190 Monthly yields (g N ha^{-1}) were calculated by dividing monthly loads by watershed area and monthly
191 flow-weighted concentrations (mg N L^{-1}) were calculated by dividing monthly loads by monthly
192 discharge. Uncertainty of NO_3^- Total was estimated using block bootstrapping methods for WRTDS-K
193 (Zhang and Hirsch, 2019) and was propagated through all analyses using NO_3^- Total loads and/or yields.

194 2.6 Terrestrial $\delta^{18}\text{O}$ and $\delta^{15}\text{N}$ calculation

195 Streamwater storm samples of $\delta^{18}\text{O}$ and $\delta^{15}\text{N}$ were corrected to remove the influence of
196 NO_3^- Atm (Dejwakh et al., 2012), which has higher $\delta^{18}\text{O}$ values and can have lower $\delta^{15}\text{N}$ values than
197 terrestrial NO_3^- (Elliott et al., 2007; Kendall et al., 2007). This was done to more carefully infer how
198 terrestrial sources of NO_3^- might change during storm events, and it uses the following equations:

$$199 \quad \delta^{15}N_{Terr} = \frac{(\delta^{15}N_{Stream} - \delta^{15}N_{Atm} \times f_{Atm})}{f_{Terr}} \quad (\text{eq. 7})$$

$$201 \quad \delta^{18}O_{Terr} = \frac{(\delta^{18}O_{Stream} - \delta^{18}O_{Atm} \times f_{Atm})}{f_{Terr}}$$

$$200 \quad (\text{eq. 8})$$

202 where $\delta^{15}\text{N}/\delta^{18}\text{O}_{Stream}$ = measured $\delta^{15}\text{N}$ or $\delta^{18}\text{O}$ of streamwater storm samples, $\delta^{15}\text{N}/\delta^{18}\text{O}_{Atm}$ = rainfall
203 $\delta^{15}\text{N}$ or $\delta^{18}\text{O}$ for a given event, f_{Atm} = fraction of NO_3^- Atm, as calculated using eq. 2, and $f_{Terr} = 1 - f_{Atm}$.

204 2.7 Hydrograph separation

205 Water isotopes were used to quantify the proportion of event and pre-event water during
206 storm events at or near peak discharge. The direct routing, or translation of rainfall to streamwater
207 during the same event, was quantified as the event-water fraction (i.e., rainfall), whereas water present
208 in the catchment prior to the storm event was classified as the pre-event water fraction (i.e., baseflow)
209 using the following equations (Sklash et al., 1976):

$$210 \quad f_{Event\ Water} + f_{Pre-Event\ Water} = 1 \quad (\text{eq. 9})$$

$$211 \quad f_{Event\ Water} = \frac{\delta^{18}O_{PeakQ} - \delta^{18}O_{Baseflow}}{\delta^{18}O_{Precipitation} - \delta^{18}O_{Baseflow}} \quad (\text{eq. 10})$$



212 where $\delta^{18}\text{O}_{\text{PeakQ}} = \delta^{18}\text{O}_{\text{H}_2\text{O}}$ at or near peak discharge during storm events, $\delta^{18}\text{O}_{\text{Baseflow}} = \delta^{18}\text{O}_{\text{H}_2\text{O}}$ of
213 streamwater just prior to storm event and hydrograph rise, and $\delta^{18}\text{O}_{\text{Rainfall}} = \delta^{18}\text{O}_{\text{H}_2\text{O}}$ of bulk rainfall
214 samples during a given storm event. Event and pre-event water runoff can be quantified using these
215 equations by multiplying runoff during peak stormflow by fractions of event and pre-event water.
216 Uncertainty was estimated using published methods to account for analytical uncertainty and
217 separation, or lack thereof, of end-members (Genereux, 1998). It has been shown that some of the
218 assumptions of isotope-based hydrograph separation may be violated in mesoscale catchments (e.g.,
219 spatiotemporally constant end-member values; Klaus and McDonnell, 2013), thus we estimate event-
220 water fractions and runoff for peak discharge only and apply these data cautiously.

221 2.8 Framework for interpreting baseflow and stormflow contributions

222 The importance of storm events relative to baseflow in streamwater NO_3^- export can be
223 evaluated using a fractional export plot (Figure 2). In this plot the y-axis shows the fraction of annual
224 nitrate loads exported during a single event (f_{NO_3}) and the x-axis shows the fraction of annual discharge
225 exported during a single event (f_{Runoff}). For example, if NO_3^- concentrations remain constant with
226 changing discharge during a storm, the data would fall on the 1:1 line because its load is perfectly
227 explained by discharge and both storm events and baseflow have equal impact on loads (Figure 2). If
228 NO_3^- concentrations decrease with increasing discharge during a storm, the data would plot below the
229 1:1 line. Watersheds with events consistently plotting below the 1:1 line indicate that baseflow, relative
230 to storm events, has an outsized impact on riverine nitrate loads. If NO_3^- concentrations increase with
231 increasing discharge, the data would plot above the 1:1 line. Watersheds with events consistently
232 plotting above the 1:1 line indicate that storm events have an outsized impact on riverine NO_3^- loads.
233 This framework can be expanded further by quantifying the (potential) disproportionate effect of storm
234 events on streamwater constituent loads relative to water yields. Dividing f_{NO_3} by f_{Runoff} provides a
235 single value to quantify the level of disproportionality:

$$236 \quad \text{Disproportionality Factor (DF)} = \frac{f_{\text{NO}_3}}{f_{\text{Runoff}}} \quad (\text{eq. 11})$$

237 DF can be interpreted using Figure 2: a value falling on the 1:1 line would have $DF = 1$, a value below
238 the 1:1 line would have a $DF < 1$, and a value above the 1:1 line would have $DF > 1$. For example, an



239 event with $DF = 4$ indicates that a given storm exported $4\times$ more NO_3^- than water whereas an event
240 with $DF = 0.5$ indicates that a storm exported.

241 2.9 Statistical analyses

242 All statistical tests were performed in R (R Development Core Team, 2019). A Wilcoxon
243 ranked-sum test was used to compare EMC and EMV of paired streamwater storm and baseflow
244 samples. Due to the presence of outliers, Theil-Sen slopes (calculated using the *sen* function in R)
245 were used to assess relationships between most continuous variables (Helsel et al., 2020). Least
246 squares linear regression was used when outliers were absent. Confidence intervals (95%) and p-values
247 of Theil-Sen slopes were computed using bootstrapping (10,000 replicates) to incorporate uncertainty
248 in DF and event-water fractions.

249 3 Results

250 Rainfall depth and chemistry (NO_3^- concentrations and isotopes, H_2O isotopes) were similar
251 between watersheds for sampled events ($p > 0.1$, Table S1). Rainfall depths ranged from 1.90 – 8.10
252 cm, which corresponds to a range of 24-hour precipitation depth return intervals of <1 year (1-year
253 return interval ≈ 6.75 cm) up to 2-year (2-year return interval ≈ 8.3 cm) in this region (Bonnin et al.,
254 2004). Streamwater NO_3^- concentrations ranged from 0.05 – 0.26 mg N L^{-1} , $\delta^{15}\text{N-NO}_3^-$ from -8.7 – -
255 1.4 ‰, $\delta^{18}\text{O-NO}_3^-$ from 48.0 – 69.6 ‰, and $\Delta^{17}\text{O-NO}_3^-$ from 13.6 – 24.9 ‰. Streamflow was slightly
256 more variable in GWN during storm events (Table S2): event mean runoff and event maximum runoff
257 were higher in GWN ($p < 0.05$ and $p < 0.01$ respectively), but event median runoff was not different
258 between the watersheds ($p = 0.11$). Across all flow conditions, NO_3^- concentrations were lower at
259 GWN (median = 0.78 mg N L^{-1}) than GUN (median = 2.60 mg N L^{-1}). Baseflow NO_3^- concentrations
260 were higher than stormflow NO_3^- EMCs in both watersheds, but differences were more pronounced at
261 GWN (baseflow median = 1.79 mg N L^{-1} , storm median = 0.66 mg N L^{-1} , $p < 0.05$) than GUN
262 (baseflow median = 3.06 mg N L^{-1} , storm median = 2.55 mg N L^{-1} , $p < 0.05$, Figure 3 and Table S3).

263 At GWN, values of $\delta^{15}\text{N}$ were higher in baseflow (median $\delta^{15}\text{N} = 7.6$ ‰) than stormflow
264 (EMV median $\delta^{15}\text{N} = 5.0$ ‰, respectively, $p < 0.05$), whereas values of $\delta^{18}\text{O-NO}_3^-$ were lower in
265 baseflow (median $\delta^{18}\text{O} = 3.9$ ‰) than stormflow (EMV median $\delta^{18}\text{O} = 7.4$ ‰, $p < 0.05$). In contrast,



266 values of $\delta^{15}\text{N}$ - and $\delta^{18}\text{O}\text{-NO}_3^-$ did not differ between baseflow and stormflow at GUN (baseflow
267 median $\delta^{15}\text{N} = 6.2 \text{ ‰}$, $\delta^{18}\text{O} = 3.3 \text{ ‰}$; stormflow EMV median $\delta^{15}\text{N} = 6.1 \text{ ‰}$, $\delta^{18}\text{O} = 3.0 \text{ ‰}$; Figure 3
268 and Table S3). Values of $\delta^{18}\text{O}\text{-NO}_3^-_{\text{Terr}}$ were higher during baseflow at both sites ($p < 0.05$, Figure 3),
269 whereas $\delta^{15}\text{N}\text{-NO}_3^-_{\text{Terr}}$ was higher during baseflow at GWN only ($p < 0.05$, Figure 3). Similarly, $\Delta^{17}\text{O}$
270 of NO_3^- was not significantly different between baseflow (median = 0.4 ‰) and stormflow (EMV
271 median = 0.5 ‰) at GUN, but was lower during baseflow (median = 0.7 ‰) than stormflow (EMV
272 median = 2.0 ‰ , $p < 0.05$, Figure 3 and Table S3) at GWN.

273 Concentrations of $\text{NO}_3^-_{\text{Terr}}$ were more temporally variable than $\text{NO}_3^-_{\text{Atm}}$. Concentrations of
274 $\text{NO}_3^-_{\text{Terr}}$ showed similar patterns to $\text{NO}_3^-_{\text{Total}}$ at both watersheds: higher during baseflow than storm
275 events (GWN baseflow median = 1.72 mg N L^{-1} , stormflow median = 0.59 mg N L^{-1} ; $p < 0.001$, GUN
276 baseflow median = 3.03 mg N L^{-1} , stormflow median = 2.50 mg N L^{-1} ; $p < 0.005$, Figure S3). Both
277 GWN and GUN had similar $\text{NO}_3^-_{\text{Atm}}$ concentrations between baseflow and storm events (GWN
278 baseflow median = 0.05 mg N L^{-1} , stormflow median = 0.06 mg N L^{-1} , $p > 0.05$, GUN baseflow
279 median = 0.04 mg N L^{-1} , stormflow median = 0.06 mg N L^{-1} , $p > 0.05$, Figure S3).

280 Similar to NO_3^- concentrations and isotopes, $\delta^{18}\text{O}\text{-H}_2\text{O}$ values exhibited greater variability
281 between baseflow and peak streamflow in GWN than in GUN. From baseflow to approximately peak
282 streamflow, $\delta^{18}\text{O}\text{-H}_2\text{O}$ shifted by an absolute average of 2.1 ‰ at GWN but only 0.6 ‰ at GUN (Table
283 S2). These shifts correspond to an average event-water fraction at peak storm discharge of 0.75 ± 0.13
284 at GWN and 0.27 ± 0.23 at GUN (Table S2). Event-water fraction uncertainty was relatively large for
285 several events due to small separation between $\delta^{18}\text{O}\text{-H}_2\text{O}$ end members. For example, rainfall and pre-
286 event baseflow end members were separated by only 0.5 ‰ during the 7/22/19 event at GUN, resulting
287 in uncertainty of event-water fractions exceeding 1 (Tables S1 and S2).

288 Storms events have an outsized impact, relative to baseflow, on $\text{NO}_3^-_{\text{Atm}}$ export at GWN, as
289 indicated by $DF > 1$ for 7 of 8 sampled events (mean = 2.6 ± 0.4 ; Figure 2). The opposite relationship
290 was observed for $\text{NO}_3^-_{\text{Terr}}$ at GWN ($DF \leq 1$ for all sampled events, mean = 0.5 ± 0.1) indicating that
291 baseflow has an outsized impact on $\text{NO}_3^-_{\text{Terr}}$ loads relative to storm events. Conversely, DF values at
292 GUN were approximately 1 for both $\text{NO}_3^-_{\text{Atm}}$ (mean = 1.1 ± 0.2) and $\text{NO}_3^-_{\text{Terr}}$ (mean = 1.0 ± 0.1),
293 indicating that neither baseflow nor stormflow disproportionately impacted stream NO_3^- loads (Figure



294 2). Event-water fractions were positively, though not significantly, related to DF of $\text{NO}_3^-_{\text{Atm}}$ ($\tau = 0.32$,
295 $p = 0.09$) and negatively related to DF of $\text{NO}_3^-_{\text{Terr}}$ across both watersheds (Figure 4; $\tau = -0.32$, $p <$
296 0.05). In GWN, the total rainfall depth for a given event was positively correlated with the fraction of
297 deposited NO_3^- that was exported in streamwater during the same event ($\tau = 0.74$, $p < 0.05$), but there
298 was no relationship for GUN (Figure 5). Additionally, there was a 1:1 relationship between the event
299 $\text{NO}_3^-_{\text{Atm}}$ deposition on impervious surfaces and the event $\text{NO}_3^-_{\text{Atm}}$ streamwater export at GWN ($r^2 =$
300 0.55 , $p < 0.05$), but not at GUN (Figure 6). $\text{NO}_3^-_{\text{Atm}}$ load estimates using traditional methods
301 (concentration from a single grab sample multiplied by mean daily discharge) were biased (range = -
302 197 % – 123 %, median absolute value = 36 %) relative to $\text{NO}_3^-_{\text{Atm}}$ load estimates using the multiple
303 samples we collected across the storm hydrograph for the two events that encompassed a full day.

304 4 Discussion

305 Hydrologic effects of impervious surfaces likely drive the disproportionate impact of storm
306 events on $\text{NO}_3^-_{\text{Atm}}$, and of baseflow on $\text{NO}_3^-_{\text{Terr}}$, in the more developed watershed (GWN). Impervious
307 surfaces increase peak storm runoff (Arnold and Gibbons, 1996; Walsh et al., 2005), but differences in
308 peak discharge alone are not the sole explanation for the contrasting results of DF for $\text{NO}_3^-_{\text{Terr}}$ and
309 $\text{NO}_3^-_{\text{Atm}}$ between the watersheds. Sampled events with overlapping f_{Runoff} between sites (i.e., similar x-
310 axis values on Figure 2) indicate that the difference between f_{NO_3} for $\text{NO}_3^-_{\text{Terr}}$ and $\text{NO}_3^-_{\text{Atm}}$ is much
311 greater at the more developed (GWN) than the less developed watershed (GUN; i.e., different y-axis values
312 on Figure 2). Thus, it is the overland routing of rainfall, and $\text{NO}_3^-_{\text{Atm}}$ dissolved therein, that likely
313 contributes to the outsized impact of storm events on $\text{NO}_3^-_{\text{Atm}}$ in the developed watershed. Although
314 both watersheds show a positive relationship between event-water fractions and DF of $\text{NO}_3^-_{\text{Atm}}$ ($p =$
315 0.09 , Figure 4), event-water fractions are much greater in the more developed watershed, GWN (green
316 triangles in Figure 4). Higher event-water fractions promote greater export of $\text{NO}_3^-_{\text{Atm}}$ by reducing the
317 potential for biological processing or retention. Our results provide evidence (i.e., increased event-
318 water fractions, proportional streamwater export of impervious $\text{NO}_3^-_{\text{Atm}}$ deposition) for the mechanism
319 (i.e., direct routing of rainfall $\text{NO}_3^-_{\text{Atm}}$ to streams) that generates increased $\text{NO}_3^-_{\text{Atm}}$ export in more
320 developed watersheds, which thus expands on previous research demonstrating that more developed



321 watersheds export relatively more $\text{NO}_3^-_{\text{Atm}}$ (Buda and DeWalle, 2009; Burns et al., 2009; Kaushal et
322 al., 2011; Bostic et al., 2021).

323 Our study collected samples across the storm hydrograph and measured $\Delta^{17}\text{O}$ of NO_3^- , which
324 provided a more accurate load estimates of, and insights into, storm $\text{NO}_3^-_{\text{Atm}}$ export than $\delta^{18}\text{O}$ of
325 NO_3^- . For example, estimates of daily $\text{NO}_3^-_{\text{Atm}}$ loads were biased by a median absolute value of 36%
326 using standard methods (i.e., daily average discharge multiplied by $\text{NO}_3^-_{\text{Atm}}$ concentration, estimated
327 using $\Delta^{17}\text{O}$, of a single grab sample; Tsunogai et al., 2014; Rose et al., 2015b; Nakagawa et al., 2018)
328 when compared to “true” daily loads calculated using samples collected across the storm hydrograph
329 from two events that encompassed a full day. Additionally, use of $\Delta^{17}\text{O}$ generally provides more
330 certain estimates of $\text{NO}_3^-_{\text{Atm}}$ fractions and concentrations than $\delta^{18}\text{O}$ because biological processing
331 (e.g., assimilation, denitrification) can change the $\delta^{18}\text{O}$ of NO_3^- and generate large uncertainty (\pm
332 $\sim 30\%$, Kendall et al., 2007) in the $\delta^{18}\text{O}\text{-NO}_3^-_{\text{Ter}}$ end-member and ultimately estimates of $\text{NO}_3^-_{\text{Atm}}$
333 (Tsunogai et al., 2016). $\Delta^{17}\text{O}$ of NO_3^- , due to its mass-independent fractionation origin, is not subject
334 to the same variability associated with biological processing as $\delta^{18}\text{O}$, thereby decreasing uncertainty in
335 $\text{NO}_3^-_{\text{Atm}}$ estimates (Young et al., 2002; Michalski et al., 2004; Kendall et al., 2007). Indeed, average
336 event $\text{NO}_3^-_{\text{Atm}}$ fractions (i.e., $\frac{\text{NO}_3^-_{\text{Atm}}}{\text{NO}_3^-_{\text{Total}}}$) would have been underestimated by an average of 3% (range = 0
337 – 7 %) at both sites if using $\delta^{18}\text{O}\text{-NO}_3^-$ only (Figure S4), but with a greater effect at the more
338 developed site (GWN). An average underestimate of 3% may appear minor, but it is notable
339 considering that event $\text{NO}_3^-_{\text{Atm}}$ fractions averaged 2% and 10% in the less and more developed
340 watersheds, respectively. Increased accuracy of $\text{NO}_3^-_{\text{Atm}}$ export during storm events combined with the
341 *DF* conceptual framework (Figure 2) provides a relatively simple means of assessing whether storm
342 events or baseflow have an outsized impact on NO_3^- source export. More accurate estimates of
343 $\text{NO}_3^-_{\text{Atm}}$ export also allow for more quantitative investigations into the role of impervious surfaces in
344 routing event rainfall $\text{NO}_3^-_{\text{Atm}}$ to streams.

345 Impervious areas in the developed watershed are effective conduits of $\text{NO}_3^-_{\text{Atm}}$ to surface
346 waters, as demonstrated by the approximately proportional relationship between event streamwater
347 $\text{NO}_3^-_{\text{Atm}}$ export and event $\text{NO}_3^-_{\text{Atm}}$ deposition on impervious surfaces (Figure 6). This relationship



348 provides evidence, in addition to higher event-water fractions (Figure 4), for the mechanism of
349 impervious surfaces enhancing export of $\text{NO}_3^-_{\text{Atm}}$ during storm events. The 1:1 correspondence of this
350 relationship is surprising, however. For 100% of rainfall $\text{NO}_3^-_{\text{Atm}}$ on impervious surfaces to be
351 exported as streamwater during a given event (i.e., 1:1 relationship), all impervious area in the
352 watershed would have to be hydrologically connected to surface waters (i.e., effective impervious
353 areas; Shuster et al., 2005). In a mesoscale (84 km²) and heterogeneous watershed such as GWN, the
354 total impervious area is not equivalent to effective impervious area. Rather, many impervious surfaces
355 drain onto pervious surfaces, or are “ineffective” at directly routing precipitation to channels (Walesh,
356 1989; but we note that certain pervious surfaces, such as reclaimed mine lands, effectively function as
357 impervious, e.g., Negley and Eshleman 2006). It is likely that the observed 1:1 relationship (Figure 6)
358 is additionally affected by flushing of dry $\text{NO}_3^-_{\text{Atm}}$ deposition from effective impervious areas. Dry
359 NO_3^- deposition, similar to wet deposition, inherits positive $\Delta^{17}\text{O}$ values (~15 – 30 ‰; Nelson et al.,
360 2018) and is generally higher in urban relative to rural areas both locally (Lovett et al., 2000; Bettez
361 and Groffman, 2013) and globally (Decina et al., 2019). Thus, flushing of dry NO_3^- deposition residing
362 on impervious surfaces (or on surfaces such as leaves that can wash onto impervious surfaces) during
363 storm events could contribute to the 1:1 relationship observed in the more developed watershed (green
364 circles in Figure 6).

365 $\Delta^{17}\text{O}$ of NO_3^- can additionally be used to “correct” $\delta^{15}\text{N}$ and $\delta^{18}\text{O}$ values (eqs. 7 and 8) to
366 better indicate isotope values of terrestrial NO_3^- sources (Dejwakh et al., 2012). Values of both
367 $\delta^{15}\text{N}_{\text{Terr}}$ and $\delta^{18}\text{O}-\text{NO}_3^-_{\text{Terr}}$ during storm events fall within the range of values that are typical of natural
368 “soil” and fertilizer (Kendall et al., 2007), but interestingly, $\text{NO}_3^-_{\text{Terr}}$ isotope values decreased during
369 storm events relative to baseflow in both watersheds (though not significantly for $\delta^{15}\text{N}$ in GUN; Figure
370 3). This shift to lower $\delta^{15}\text{N}_{\text{Terr}}$ and $\delta^{18}\text{O}-\text{NO}_3^-_{\text{Terr}}$ values during storm events may reflect the flushing of
371 less “processed” NO_3^- sources from upper soil horizons (Creed et al., 1996), as processing (e.g.,
372 denitrification) generally leaves the remaining NO_3^- with more positive $\delta^{15}\text{N}$ and $\delta^{18}\text{O}$ values due to
373 biologically-mediated fractionation (Denk et al., 2017). Impervious surfaces in the developed
374 watershed likely reduce flushing of this lower $\delta^{18}\text{O}-\text{NO}_3^-_{\text{Terr}}$ by restricting infiltration, but 30% of this
375 watershed is not “developed” (and a higher percentage contains pervious surfaces), which likely



376 contributes to the similarity in NO_3^- Terr isotope patterns between study watersheds. Relatively lower
377 $\delta^{18}\text{O}$ - NO_3^- Terr values during storm events relative to baseflow, and associated insights into watershed-
378 scale N biogeochemistry, were only realized by using $\Delta^{17}\text{O}$ to “correct” $\delta^{18}\text{O}$ values. Without this
379 correction, $\delta^{18}\text{O}$ - NO_3^- during storm events is strongly influenced by elevated $\delta^{18}\text{O}$ of NO_3^- Atm, as
380 shown by the similar patterns between $\Delta^{17}\text{O}$ and “uncorrected” $\delta^{18}\text{O}$ in the more developed watershed
381 (Figure 3).

382 Large inputs and stores of N associated with agricultural activity likely contribute to baseflow
383 and storm events having similar impacts on NO_3^- Terr and NO_3^- Atm export in the mixed
384 agricultural/forested watershed (GUN). *DFs* of both NO_3^- Terr and NO_3^- Atm were approximately 1,
385 indicating that loads are primarily explained by changes in discharge. Nutrients, including NO_3^- ,
386 showing similar patterns (loads explained primarily by discharge) over annual time-scales have been
387 attributed to large stores of NO_3^- associated with agricultural inputs (Basu et al., 2010; Thompson et
388 al., 2011). With significant agricultural land-use, both currently (41.3% in 2016; Table 1) and
389 historically (~58% in 1960; O’Bryan and McAvoy, 1966), and consistently high NO_3^- concentrations
390 in streamwater, GUN likely has large stores of NO_3^- in soil and groundwater. Interestingly, our results
391 demonstrate the control of discharge on NO_3^- Terr and NO_3^- Atm loads over storm-event time scales,
392 suggesting that large reservoirs of NO_3^- contribute to streamwater export of nutrients across varied
393 flow conditions and not just baseflow.

394 The combination of our results with projections of increasing frequency of intense
395 precipitation events (Najjar et al., 2010; Walsh et al., 2014) and increasing urban and suburban sprawl
396 (Jantz et al., 2005; Seto et al., 2012) suggest that NO_3^- Atm may become a relatively more important
397 NO_3^- source to downstream waters, assuming no change in NO_3^- deposition rates. This assumption
398 may not be valid everywhere, however; for example, NO_3^- deposition is declining locally (i.e., mid-
399 Atlantic USA; Li et al., 2016) but increasing across many regions (i.e., east Asia; Liu et al., 2013). In
400 our more developed watershed, the positive correlation between rainfall and the fraction of deposited
401 NO_3^- exported in streamwater (Figure 5) suggests that large storm events may export proportionally
402 greater fractions of rainfall NO_3^- Atm in urbanizing catchments and increased loads of NO_3^- Atm to
403 downstream waters. Best management practices in developed watersheds (e.g., stormwater control



404 measures) can mitigate these potential impacts by increasing infiltration of rainfall (and NO_3^-
405 dissolved in rainfall) and reducing hydrologic connectivity of overland flowpaths (i.e., decrease
406 effective impervious areas; Lee and Heaney, 2003; Walsh et al., 2009), both of which may reduce the
407 load of $\text{NO}_3^-_{\text{Atm}}$ and the proportion of “event” water in streams during storm events. Such practices
408 may additionally reduce $\text{NO}_3^-_{\text{Terr}}$ loads by stimulating denitrification (Bettez and Groffman, 2012), but
409 could also increase the importance of baseflow in NO_3^- export due to increased infiltration. Thus,
410 monitoring of both baseflow and storm events is necessary to quantify potential changes and make
411 targeted water-quality management decisions. Finally, best management practices intended to reduce
412 $\text{NO}_3^-_{\text{Atm}}$ loads in developed watersheds via increased infiltration may provide numerous co-benefits,
413 including reduced runoff (Hood et al., 2007) and higher baseflow (Fletcher et al., 2013), both of which
414 could help restore aquatic ecosystems impacted by urbanization (Walsh et al., 2005).

415 **5. Conclusion**

416 We found that stormflow has a disproportionately large impact on $\text{NO}_3^-_{\text{Atm}}$ export whereas
417 baseflow has a disproportionately small impact on $\text{NO}_3^-_{\text{Terr}}$ export in a moderately developed
418 watershed. In contrast, neither stormflow nor baseflow have an outsized impact on $\text{NO}_3^-_{\text{Atm}}$ or
419 $\text{NO}_3^-_{\text{Terr}}$ export in a mixed land-use watershed with significant agriculture. Hydrologic connectivity of
420 overland flow paths associated with impervious surfaces likely promote rapid transport of $\text{NO}_3^-_{\text{Atm}}$ to
421 streams during storm events in the more developed watershed, with higher rainfall storms exporting a
422 greater fraction of deposited NO_3^- than lower rainfall events and event $\text{NO}_3^-_{\text{Atm}}$ streamwater export
423 approximately equaling rainfall $\text{NO}_3^-_{\text{Atm}}$ on impervious surfaces. Large reserves of new and/or legacy
424 agricultural-associated nitrogen in soils in the mixed land-use watershed likely influenced the similar
425 response of $\text{NO}_3^-_{\text{Atm}}$ or $\text{NO}_3^-_{\text{Terr}}$ to stormflow and baseflow.

426 **Appendices**

427 Not applicable.



428 **Code availability**

429 Not applicable.

430 **Data availability**

431 Available upon request.

432 **Author contributions**

433 DMN and KNE: Conceptualization, Methodology, Writing – Review and Editing, Supervision,

434 Funding Acquisition

435 JTB: Conceptualization, Methodology, Investigation, Formal Analysis, Writing – Original Draft,

436 Writing – Review and Editing, Visualization, Funding Acquisition



Acknowledgements

Thanks to Pavithra Pitumpe Arachchige and Jim Garlitz for NO_3^- concentration analysis. Robert Hirsch of the U.S. Geological Survey provided guidance on WRTDS-K and R scripts for estimating $\text{NO}_{3\text{-Total}}$ uncertainty. DMN, KNE, and JTB received support from Maryland Sea Grant under award NA14OAR4170090 R/WS-3 from the National Oceanic and Atmospheric Administration, U.S. Department of Commerce. JTB received support from Maryland Sea Grant under award SA75281900-A from the National Oceanic and Atmospheric Administration, U.S. Department of Commerce. This material is based upon work supported by the National Science Foundation Graduate Research Fellowship (to JTB) under Grant No. 1840380. Any opinion, findings, conclusions, recommendations expressed in this material are those of the authors and do not necessarily reflect the views of the National Science Foundation.

References

- Arnold CL, Gibbons CJ. 1996. Impervious surface coverage: The emergence of a key environmental indicator. *Journal of the American Planning Association* 62: 243-258. <https://doi.org/10.1080/01944369608975688>
- Barnes RT, Raymond PA. 2010. Land-use controls on sources and processing of nitrate in small watersheds: Insights from dual isotopic analysis. *Ecological Applications* 20: 1961-1978. <https://doi.org/10.1890/08-1328.1>
- Basu NB, Destouni G, Jawitz JW, Thompson SE, Loukinova NV, Darracq A, Zanardo S, Yaeger M, Sivapalan M, Rinaldo A, Rao PSC. 2010. Nutrient loads exported from managed catchments reveal emergent biogeochemical stationarity. *Geophysical Research Letters* 37. <https://doi.org/10.1029/2010GL045168>
- Bettez N, Groffman P. 2012. Denitrification potential in stormwater control structures and natural riparian zones in an urban landscape. *Environmental Science & Technology* 46 20: 10909-10917. <https://doi.org/10.1021/es301409z>
- Bettez ND, Groffman PM. 2013. Nitrogen deposition in and near an urban ecosystem. *Environmental Science & Technology* 47: 6047-6051. <https://doi.org/10.1021/es400664b>
- Böhlke JK, Mroczkowski SJ, Coplen TB. 2003. Oxygen isotopes in nitrate: New reference materials for ^{18}O : ^{17}O : ^{16}O measurements and observations on nitrate-water equilibration. *Rapid Communications in Mass Spectrometry* 17: 1835-1846. <https://doi.org/10.1002/rcm.1123>



Bonnin GM, Martin D, Lin B, Parzybok T, Yekta M, Riley D. 2004. Precipitation-frequency atlas of the United States. Volume 2 version 3.0. Delaware, District of Columbia, Illinois, Indiana, Kentucky, Maryland, New Jersey, North Carolina, Ohio, Pennsylvania, South Carolina, Tennessee, Virginia, West Virginia.

Bostic JT, Nelson DM, Sabo RD, Eshleman KN. 2021. Terrestrial nitrogen inputs affect the export of unprocessed atmospheric nitrate to surface waters: Insights from triple oxygen isotopes of nitrate. *Ecosystems*.
<https://doi.org/10.1007/s10021-021-00722-9>

Buda AR, DeWalle DR. 2009. Dynamics of stream nitrate sources and flow pathways during stormflows on urban, forest and agricultural watersheds in central Pennsylvania, USA. *Hydrological Processes* 23: 3292-3305.
<https://doi.org/10.1002/hyp.7423>

Burns DA, Boyer EW, Elliott EM, Kendall C. 2009. Sources and transformations of nitrate from streams draining varying land uses: Evidence from dual isotope analysis. *Journal of Environmental Quality* 38: 1149-1159.
10.2134/jeq2008.0371

Camargo JA, Alonso Á. 2006. Ecological and toxicological effects of inorganic nitrogen pollution in aquatic ecosystems: A global assessment. *Environment International* 32: 831-849.
<https://doi.org/10.1016/j.envint.2006.05.002>

Casciotti KL, Sigman DM, Hastings MG, Böhlke J, Hilbert A. 2002. Measurement of the oxygen isotopic composition of nitrate in seawater and freshwater using the denitrifier method. *Analytical Chemistry* 74: 4905-4912.
<https://doi.org/10.1021/ac020113w>

Chesapeake Bay Program. 2019. Chesapeake assessment and scenario tool (CAST). Chesapeake Bay Program Office.

Chesapeake Bay Program. 2021. Chesapeake Bay Program Water Quality Database, 1984-present. Accessed March 1, 2021 from http://www.chesapeakebay.net/data/downloads/cbp_water_quality_database_1984_present.

Chanat JG, Moyer DL, Blomquist JD, Hyer KE, Langland MJ. 2016. Application of a weighted regression model for reporting nutrient and sediment concentrations, fluxes, and trends in concentration and flux for the Chesapeake Bay nontidal water-quality monitoring network, results through water year 2012. *Scientific Investigations Report*. Reston, VA, p88. <https://doi.org/10.3133/sir20155133>

Cook PG, Herczeg AL. 2012. *Environmental tracers in subsurface hydrology*: Springer Science & Business Media.
<https://doi.org/10.1007/978-1-4615-4557-6>



Creed IF, Band LE, Foster NW, Morrison IK, Nicolson JA, Semkin RS, Jeffries DS. 1996. Regulation of nitrate-N release from temperate forests: A test of the N flushing hypothesis. *Water Resources Research* 32: 3337-3354. <https://doi.org/10.1029/96WR02399>

DeCicco LA, Lorenz, D., Hirsch, R.M. 2018. dataRetrieval: R packages for discovering and retrieving water data available from U.S. Federal hydrologic web services. United States Geological Survey. 10.5066/P9X4L3GE

Decina SM, Hutyra LR, Templer PH. 2019. Hotspots of nitrogen deposition in the world's urban areas: A global data synthesis. *Frontiers in Ecology and the Environment* 18: 92-100. <https://doi.org/10.1002/fee.2143>

Dejwakh NR, Meixner T, Michalski G, McIntosh J. 2012. Using ^{17}O to investigate nitrate sources and sinks in a semi-arid groundwater system. *Environmental Science & Technology* 46: 745-751. <https://doi.org/10.1021/es203450z>

Denk TRA, Mohn J, Decock C, Lewicka-Szczebak D, Harris E, Butterbach-Bahl K, Kiese R, Wolf B. 2017. The nitrogen cycle: A review of isotope effects and isotope modeling approaches. *Soil Biology and Biochemistry* 105: 121-137. <https://doi.org/10.1016/j.soilbio.2016.11.015>

Dingman SL. 1994. *Physical hydrology*. xii, 643 pp.

Divers, MT, Elliott, EM, Bain, DJ. Quantification of nitrate sources to an urban stream using dual nitrate isotopes. *Environmental Science & Technology*, 48: 10580-10587. <https://doi.org/10.1021/es404880j>

Edmund M. Hart and Kendon Bell. 2015. PRISM: Download data from the Oregon PRISM project.

Elliott EM, Kendall C, Wankel SD, Burns DA, Boyer EW, Harlin K, Bain DJ, Butler TJ. 2007. Nitrogen isotopes as indicators of NO_x source contributions to atmospheric nitrate deposition across the midwestern and northeastern United States. *Environmental Science & Technology* 41: 7661-7667. <https://doi.org/10.1021/es070898t>

Fenneman NM, Johnson, D.W. 1946. *Physiographic divisions of the conterminus U.S.* U.S. Geological Survey. Reston, VA.

Fletcher, T., Andrieu, H., Hamel, P. 2013. Understanding, management and modelling of urban hydrology and its consequences for receiving waters: A state of the art. *Advances in Water Resources* 51: 261-279. <https://doi.org/10.1016/j.advwatres.2012.09.001>

Genereux D. 1998. Quantifying uncertainty in tracer-based hydrograph separations. *Water Resources Research* 34: 915-919. <https://doi.org/10.1029/98WR00010>



Helsel DR, Hirsch RM, Ryberg KR, Archfield SA, Gilroy EJ. 2020. Statistical methods in water resources. Techniques and Methods. Reston, VA, p. 484. <https://doi.org/10.3133/tm4A3>

Homer C, Dewitz J, Jin S, Xian G, Costello C, Danielson P, Gass L, Funk M, Wickham J, Stehman S, Auch R, Riitters K. 2020. Conterminous united states land cover change patterns 2001–2016 from the 2016 national land cover database. *ISPRS Journal of Photogrammetry and Remote Sensing* 162: 184-199. <https://doi.org/10.1016/j.isprsjprs.2020.02.019>

Hood, M., Clausen, J., Warner, G. 2007. Comparison of stormwater lag times for low impact and traditional residential development. *Journal of the American Water Resources Association* 43: 1036-1046. <https://doi.org/10.1111/j.1752-1688.2007.00085.x>

IAEA. 1995. Reference and intercomparison materials for stable isotopes of light elements. Vienna: International Atomic Energy Agency.

Jantz P, Goetz S, Jantz C. 2005. Urbanization and the loss of resource lands in the Chesapeake Bay watershed. *Environmental Management* 36: 808-825. <https://doi.org/10.1007>

Jarvis NJ. 2020. A review of non-equilibrium water flow and solute transport in soil macropores: Principles, controlling factors and consequences for water quality. *European Journal of Soil Science* 71: 279-302. <https://doi.org/10.1111/j.1365-2389.2007.00915.x>

Kaiser J, Hastings MG, Houlton BZ, Röckmann T, Sigman DM. 2007. Triple oxygen isotope analysis of nitrate using the denitrifier method and thermal decomposition of N₂O. *Analytical Chemistry* 79: 599-607. <https://doi.org/10.1021/ac061022s>

Kaushal SS, Groffman PM, Band LE, Elliott EM, Shields CA, Kendall C. 2011. Tracking nonpoint source nitrogen pollution in human-impacted watersheds. *Environmental Science & Technology* 45: 8225-8232. <https://doi.org/10.1021/es200779e>

Kemp WM, Boynton WR, Adolf JE, Boesch DF, Boicourt WC, Brush G, Cornwell JC, Fisher TR, Glibert PM, Hagy JD. 2005. Eutrophication of Chesapeake Bay: Historical trends and ecological interactions. *Marine Ecology Progress Series* 303: 1-29. <https://doi.org/10.3354/meps303001>

Kendall C, Elliott, E, Wankel, S. 2007. Tracing anthropogenic inputs of nitrogen to ecosystems: Blackwell Publishing. <https://doi.org/10.1002/9780470691854.ch12>

Kincaid DW, Seybold EC, Adair EC, Bowden WB, Perdrial JN, Vaughan MCH, Schroth AW. 2020. Land use and season influence event-scale nitrate and soluble reactive phosphorus exports and export stoichiometry from headwater catchments. *Water Resources Research* 56. <https://doi.org/10.1029/2020WR027361>



Klaus J, McDonnell J. 2013. Hydrograph separation using stable isotopes: Review and evaluation. *Journal of Hydrology* 505: 47-64. <https://doi.org/10.1016/j.jhydrol.2013.09.006>

Kottek M, Grieser J, Beck C, Rudolf B, Rubel F. 2006. World map of the Köppen-Geiger climate classification updated. *Meteorologische Zeitschrift* 15: 259-263. <https://doi.org/10.1127/0941-2948/2006/0130>.

Lee JG, Heaney JP. 2003. Estimation of urban imperviousness and its impacts on storm water systems. *Journal of Water Resources Planning and Management* 129: 419-426. [https://doi.org/10.1061/\(ASCE\)0733-9496\(2003\)129:5\(419\)](https://doi.org/10.1061/(ASCE)0733-9496(2003)129:5(419))

Lefcheck JS, Orth RJ, Dennison WC, Wilcox DJ, Murphy RR, Keisman J, Gurbisz C, Hannam M, Landry JB, Moore KA. 2018. Long-term nutrient reductions lead to the unprecedented recovery of a temperate coastal region. *Proceedings of the National Academy of Sciences* 115: 3658-3662. <https://doi.org/10.1073/pnas.1715798115>

Li Y, Schichtel BA, Walker JT, Schwede DB, Chen X, Lehmann CM, Puchalski MA, Gay DA, Collett JL. 2016. Increasing importance of deposition of reduced nitrogen in the United States. *Proceedings of the National Academy of Sciences* 113: 5874-5879. <https://doi.org/10.1073/pnas.1525736113>

Liu, X., Zhang, Y., Wenxuan, H., Tang, A., Shen, J., Cui, Z., Vitousek, P., Erismann, J., Goudling, K., Christie, P., Fangmeier, A., Zhang, F. 2013. Enhanced nitrogen deposition over China. *Nature* 494: 459-462. <https://doi.org/10.1038/nature11917>

Lovett GM, Traynor MM, Pouyat RV, Carreiro MM, Zhu W-X, Baxter JW. 2000. Atmospheric deposition to oak forests along an urban-rural gradient. *Environmental Science & Technology* 34: 4294-4300. <https://doi.org/10.1021/es001077q>

McGuire K, McDonnell J. 2007. Stable isotope tracers in watershed hydrology. *Stable isotopes in ecology and environmental science*, p334-374. <https://doi.org/10.1002/9780470691854.ch11>

Michalski G, Meixner T, Fenn M, Hernandez L, Sirulnik A, Allen E, Thiemens M. 2004. Tracing atmospheric nitrate deposition in a complex semiarid ecosystem using $\Delta^{17}\text{O}$. *Environmental Science & Technology* 38: 2175-2181. <https://doi.org/10.1021/es034980+>

Michalski G, Savarino J, Böhlke JK, Thiemens M. 2002. Determination of the total oxygen isotopic composition of nitrate and the calibration of a $\Delta^{17}\text{O}$ nitrate reference material. *Analytical Chemistry* 74: 4989-4993. <https://doi.org/10.1021/ac0256282>



- Michalski G, Scott Z, Kabling M, Thiemens MH. 2003. First measurements and modeling of $\Delta^{17}\text{O}$ in atmospheric nitrate. *Geophysical Research Letters* 30. <https://doi.org/10.1029/2003GL017015>
- Najjar RG, Pyke CR, Adams MB, Breitburg D, Hershner C, Kemp M, Howarth R, Mulholland MR, Paolisso M, Secor D, Sellner K, Wardrop D, Wood R. 2010. Potential climate-change impacts on the Chesapeake Bay. *Estuarine, Coastal and Shelf Science* 86: 1-20. <https://doi.org/10.1016/j.ecss.2009.09.026>
- Nakagawa F, Tsunogai U, Obata Y, Ando K, Yamashita N, Saito T, Uchiyama S, Morohashi M, Sase H. 2018. Export flux of unprocessed atmospheric nitrate from temperate forested catchments: A possible new index for nitrogen saturation. *Biogeosciences* 15: 7025-7042. <https://doi.org/10.5194/bg-15-7025-2018>
- Negley, T.L. and Eshleman, K.N. 2006. Comparison of stormflow responses of surface-mined and forested watersheds in the Appalachian Mountains, USA. *Hydrological Processes* 20: 3467-3483. <https://doi.org/10.1002/hyp.6148>
- Nelson DM, Tsunogai U, Ding D, Ohyama T, Komatsu DD, Nakagawa F, Noguchi I, Yamaguchi T. 2018. Triple oxygen isotopes indicate urbanization affects sources of nitrate in wet and dry atmospheric deposition. *Atmospheric Chemistry and Physics* 18: 6381-6392. <https://doi.org/10.5194/acp-18-6381-2018>
- NRC. 2000. *Clean coastal waters: Understanding and reducing the effects of nutrient pollution*. Washington, DC: The National Academies Press. 428p. <https://doi.org/10.17226/9812>
- O'Bryan, D., and McAvoy, R.L. 1966. *Gunpowder Fall Maryland: Uses of a water resource today and tomorrow*. Geological Survey Water-Supply Paper 1815.
- Paul MJ, Meyer JL. 2001. Streams in the urban landscape. *Annual Review of Ecology and Systematics* 32: 333-365. <https://doi.org/10.1146/annurev.ecolsys.32.081501.114040>
- PRISM Climate Group, Oregon State University, <https://prism.oregonstate.edu>, data created 4 Feb 2014, accessed 16 Dec 2020.
- R Development Core Team. 2019. *R: A language and environment for statistical computing*. Vienna, Austria: R Foundation for Statistical Computing.
- Rose LA, Sebestyen SD, Elliott EM, Koba K. 2015a. Drivers of atmospheric nitrate processing and export in forested catchments. *Water Resources Research* 51: 1333-1352. <https://doi.org/10.1002/2014WR015716>



Rose LA, Elliott EM, Adams MB. 2015b. Triple nitrate isotopes indicate differing nitrate source contributions to streams across a nitrogen saturation gradient. *Ecosystems* 18: 1209-1223. <https://doi.org/10.1007/s10021-015-9891-8>

Sabo, RD, Nelson, DM, Eshleman, KN. Episodic, seasonal, and annual export of atmospheric and microbial nitrate from a temperate forest. *Geophysical Research Letters*, 43, 2: 683-691. <https://doi.org/10.1002/2015gl066758>

Seto KC, Guneralp B, Hutyra LR. 2012. Global forecasts of urban expansion to 2030 and direct impacts on biodiversity and carbon pools. *Proceedings of the National Academy of Sciences* 109: 16083-16088. <https://doi.org/10.1073/pnas.1211658109>

Shuster WD, Bonta J, Thurston H, Warnemuende E, Smith DR. 2005. Impacts of impervious surface on watershed hydrology: A review. *Urban Water Journal* 2: 263-275. <https://doi.org/10.1080/15730620500386529>

Sigman DM, Casciotti KL, Andreani M, Barford C, Galanter M, Böhlke J. 2001. A bacterial method for the nitrogen isotopic analysis of nitrate in seawater and freshwater. *Analytical Chemistry* 73: 4145-4153. <https://doi.org/10.1021/ac010088e>

Sklash M, Farvolden R, Fritz P. 1976. A conceptual model of watershed response to rainfall, developed through the use of oxygen-18 as a natural tracer. *Canadian Journal of Earth Sciences* 13: 271-283. <https://doi.org/10.1139/e76-02>

Steffen W, Richardson K, Rockström J, Cornell SE, Fetzer I, Bennett EM, Biggs R, Carpenter SR, Vries Wd, Wit CAd, Folke C, Gerten D, Heinke J, Mace GM, Persson LM, Ramanathan V, Reyers B, Sörlin S. 2015. Planetary boundaries: Guiding human development on a changing planet. *Science* 347: 6219. <https://doi.org/10.1126/science.1259855>

Stevens CJ. 2019. Nitrogen in the environment. *Science* 363: 578-580. <https://doi.org/10.1126/science.aav8215>

Thompson SE, Basu NB, Lascrain Jr. J, Aubeneau A, Rao PSC. 2011. Relative dominance of hydrologic versus biogeochemical factors on solute export across impact gradients. *Water Resources Research* 47. <https://doi.org/10.1029/2010WR009605>

Tsunogai U, Komatsu DD, Ohyama T, Suzuki A, Nakagawa F, Noguchi I, Takagi K, Nomura M, Fukuzawa K, Shibata H. 2014. Quantifying the effects of clear-cutting and strip-cutting on nitrate dynamics in a forested watershed using triple oxygen isotopes as tracers. *Biogeosciences* 11: 5411-5424. <https://doi.org/10.5194/bg-11-5411-2014>



Tsunogai U, Miyauchi T, Ohyama T, Komatsu DD, Nakagawa F, Obata Y, Sato K, Ohizumi T. 2016. Accurate and precise quantification of atmospheric nitrate in streams draining land of various uses by using triple oxygen isotopes as tracers. *Biogeosciences* 13: 3441-3459. <https://doi.org/10.5194/bg-13-3441-2016>

U.S. Geological Survey, 2022, National Water Information System data available on the World Wide Web (USGS Water Data for the Nation), accessed [June 20, 2022], at URL [<https://waterdata.usgs.gov/usa/nwis/uv?01589300> and https://waterdata.usgs.gov/md/nwis/uv/?site_no=01582500]

Vaughan MCH, Bowden WB, Shanley JB, Vermilyea A, Sleeper R, Gold AJ, Pradhanang SM, Inamdar SP, Levia DF, Andres AS, Birgand F, Schroth AW. 2017. High-frequency dissolved organic carbon and nitrate measurements reveal differences in storm hysteresis and loading in relation to land cover and seasonality. *Water Resources Research* 53: 5345-5363. <https://doi.org/10.1002/2017WR020491>

Walesh SG. 1989. Fundamentals of urban surface water management. *Urban surface water management*, p1-51. <https://doi.org/10.1002/9780470172810.ch1>

Walsh CJ, Fletcher TD, Ladson AR. 2009. Retention capacity: A metric to link stream ecology and storm-water management. *Journal of Hydrologic Engineering* 14: 399-406. [https://doi.org/10.1061/\(ASCE\)1084-0699\(2009\)14:4\(399\)](https://doi.org/10.1061/(ASCE)1084-0699(2009)14:4(399))

Walsh CJ, Roy AH, Feminella JW, Cottingham PD, Groffman PM, Morgan RP. 2005. The urban stream syndrome: Current knowledge and the search for a cure. *Journal of the North American Benthological Society* 24: 706-723. <https://doi.org/10.1899/04-028.1>

Walsh J, Wuebbles D, Hayhoe K, Kossin J, Kunkel K, Stephens G, Thome P, Vose R, Wehner M, Willis J, Anderson D, Doney S, Feely R, Hennon P, Kharin V, Knutson T, Landerer F, Lenton T, Kennedy J, Somerville R editors. 2014. Our changing climate, climate change impacts in the united states: The third national climate assessment.

Young ED, Galy A, Nagahara H. 2002. Kinetic and equilibrium mass-dependent isotope fractionation laws in nature and their geochemical and cosmochemical significance. *Geochimica et Cosmochimica Acta* 66: 1095-1104. [https://doi.org/10.1016/S0016-7037\(01\)00832-8](https://doi.org/10.1016/S0016-7037(01)00832-8)

Zhang Q, Blomquist JD, Moyer DL, Chanut JG. 2019. Estimation bias in water-quality constituent concentrations and fluxes: A synthesis for Chesapeake Bay rivers and streams. *Frontiers in Ecology and Evolution* 7. <https://doi.org/10.3389/fevo.2019.00109>



Zhang Q, Hirsch RM. 2019. River water-quality concentration and flux estimation can be improved by accounting for serial correlation through an autoregressive model. *Water Resources Research* 55: 9705-9723. <https://doi.org/10.1029/2019WR025338>

Zhang Q, Murphy RR, Tian R, Forsyth MK, Trentacoste EM, Keisman J, Tango PJ. 2018. Chesapeake Bay's water quality condition has been recovering: Insights from a multimetric indicator assessment of thirty years of tidal monitoring data. *Science of the Total Environment* 637-638: 1617-1625. <https://doi.org/10.1016/j.scitotenv.2018.05.025>



Tables

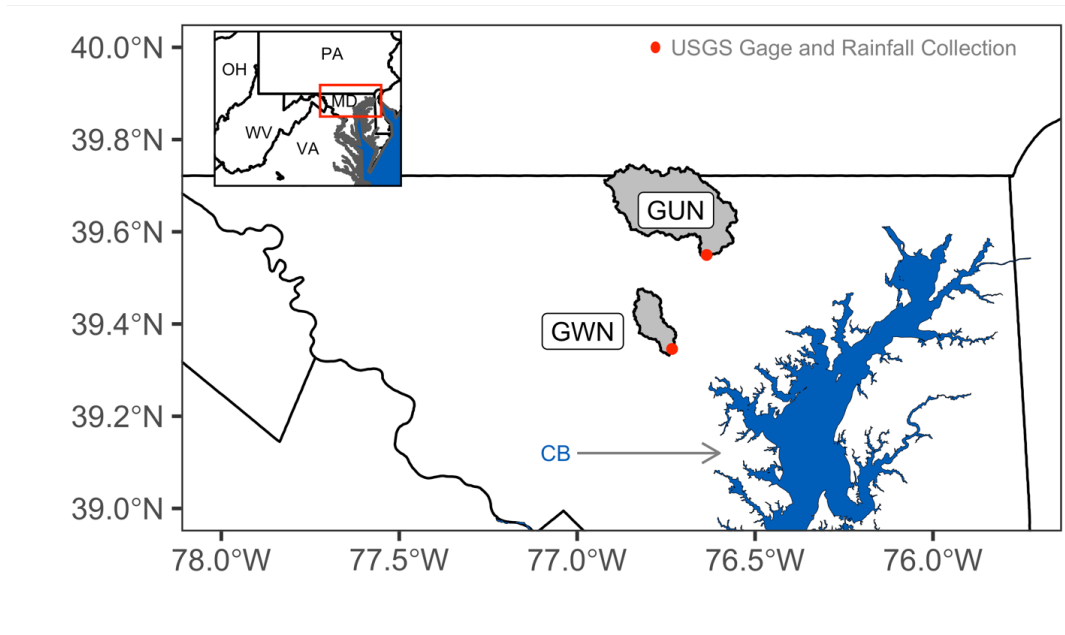
Table 1. Watershed attributes.

Watershed	Area (ha)	Land-Use (%)				MA T (°C)	MA P (cm)	Lithology (%)		
		Forest	Agriculture	Developed	Impervious			Unconsolidated	Crystalline	Carbonate
Gwynns Falls (GWN)	8400	23.4	5.0	70.1	14.6	12.7	113.5	0	95.1	4.9
Gunpowder Falls (GUN)	4140	45.4	41.3	10.9	0.3	11.9	116.0	0	99.8	0.2

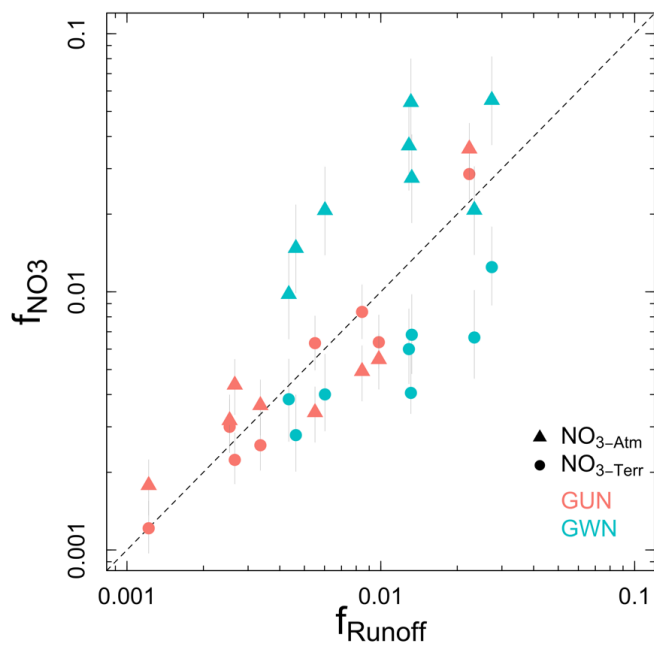
Land-use percentages were calculated from the 2016 National Land Cover Database, impervious is the sum of medium and high intensity developed land-use classes; agricultural land represents the sum of both cultivated crop and pasture/hay land classes (Homer et al., 2020). Land use percentages do not sum to 100% as all land use classes are not listed (e.g. open water, wetlands). MAT = Mean Annual Temperature, MAP = Mean Annual Precipitation. Note that MAT and MAP cover the time period from 1981-2010 (PRISM, 2014). Lithology data were obtained from Zhang et al. 2019.



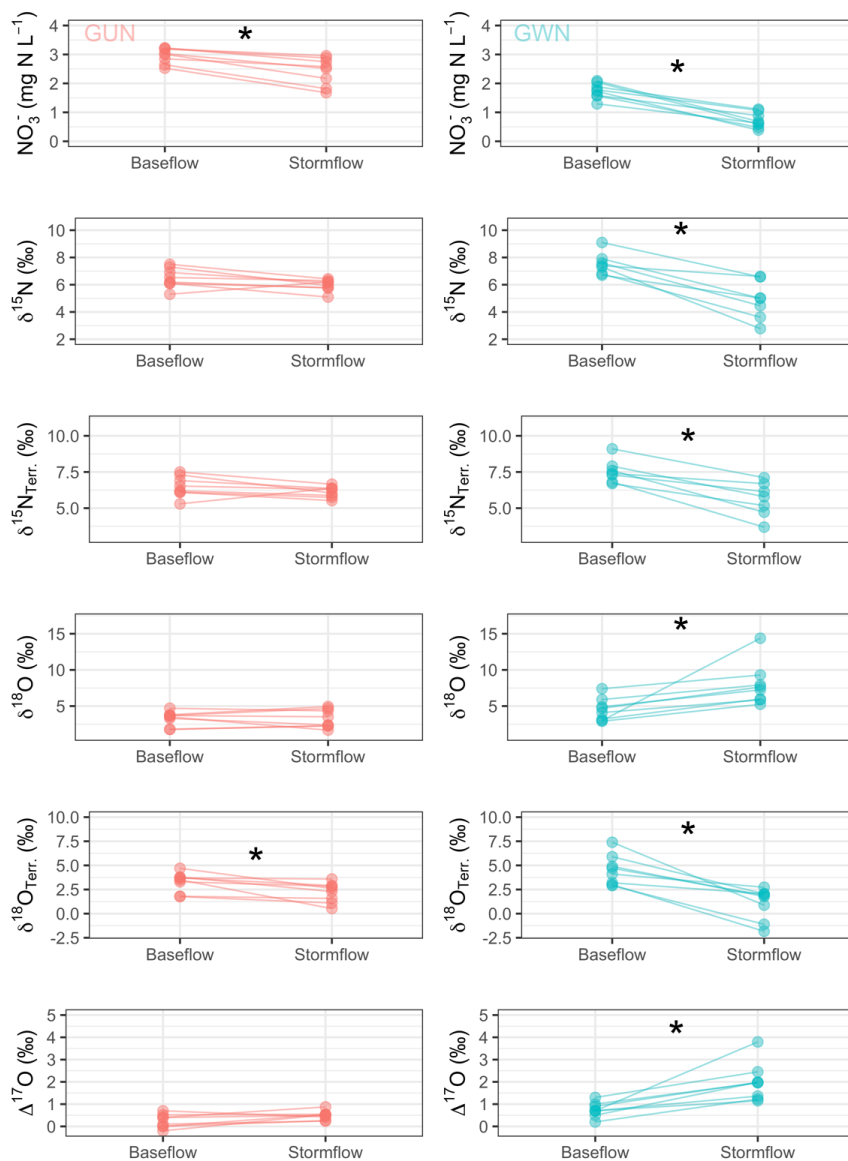
Figures



5 **Figure 1.** Site map showing watershed boundaries (GWN = Gwynns Falls, GUN = Gunpowder Falls), United States Geology Survey (USGS) gaging stations and rainfall collection sites, and Chesapeake Bay (CB) location. Inset map shows relative position of watersheds in Maryland (MD) relative to neighboring states (PA = Pennsylvania, OH = Ohio, WV = West Virginia, VA = Virginia).

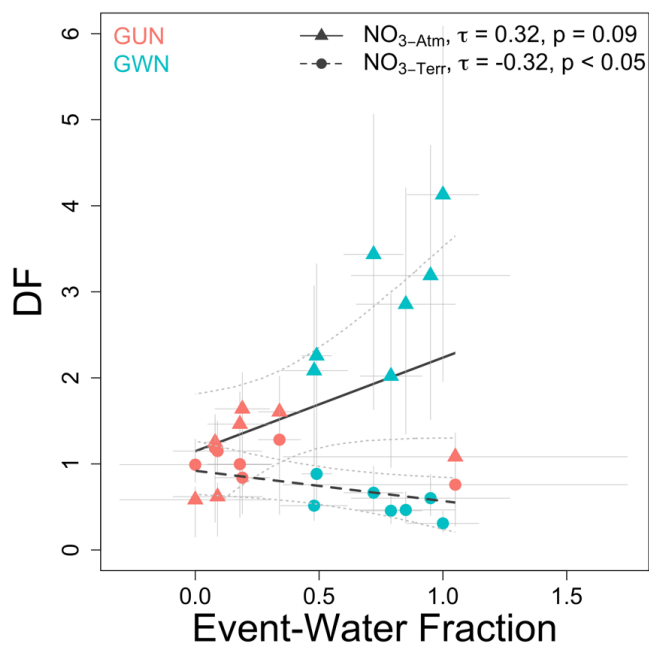


10 Figure 2. Fraction of NO_3^- loads (f_{NO_3} ; separated by NO_3^- -Terr, circles, and NO_3^- -Atm, triangles) and discharge (f_{Runoff}) during the study duration (14 months) represented by sampled storm events ($n = 8$). Points falling above the dashed line (1:1 line) indicate storm events have an outsized impact on NO_3^- loads and points falling below the line indicate baseflow has an outsized impact on NO_3^- loads. Points on or near the 1:1 line indicate a chemostatic response, in which storms nor baseflow have an outsized impact on NO_3^- loads.

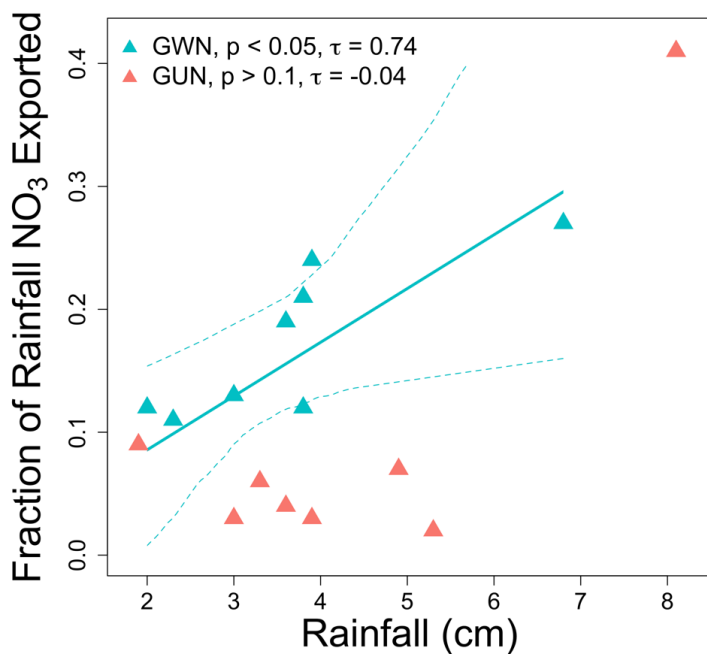


15

Figure 3. Event mean NO_3^- concentrations and $\delta^{15}\text{N}$, $\delta^{15}\text{N}_{\text{Terr.}}$, $\delta^{18}\text{O}$, $\delta^{18}\text{O}_{\text{Terr.}}$ and $\Delta^{17}\text{O}$ values of NO_3^- for samples collected during storm events paired with the corresponding baseflow sample preceding the event. Asterisk (*) indicates significant difference at $p < 0.05$ as determined using a Wilcoxon ranked-sum test.

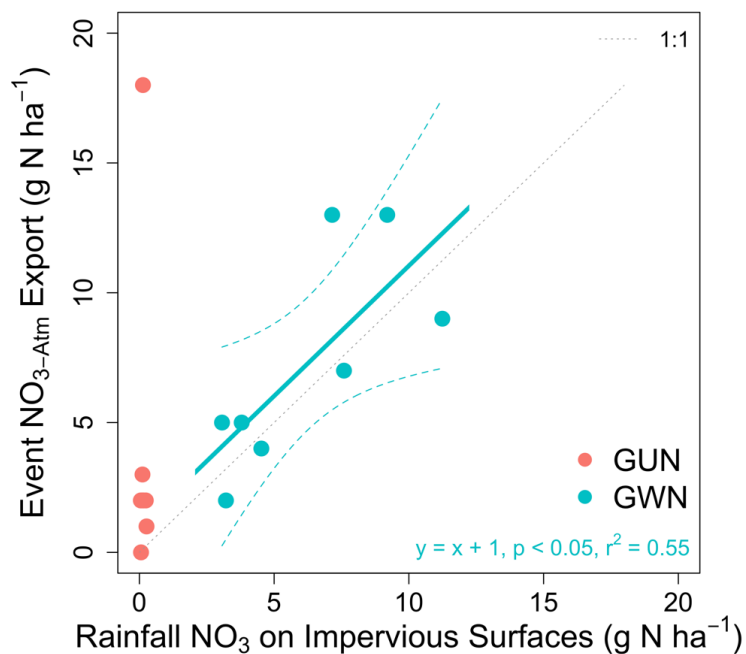


20 Figure 4. Disproportionality factor (DF) and event-water fraction for $\text{NO}_3^-_{\text{Atm}}$ (triangles) and $\text{NO}_3^-_{\text{Terr}}$ (circles). Event-water fraction and DF are positively, but not significantly correlated for $\text{NO}_3^-_{\text{Atm}}$ ($\tau = 0.32$, $p = 0.09$) while event-water fraction and DF are significantly, negative correlated for $\text{NO}_3^-_{\text{Terr}}$ ($\tau = -0.32$, $p < 0.05$) across both watersheds. The thin, dotted line shows bootstrapped 95% confidence intervals.



25

Figure 5. The fraction of NO_3^- in rainfall that is exported in streamwater during the same event is positively significantly related with total event rainfall at GWN ($p < 0.05$, $\tau = 0.74$) but not at GUN ($p > 0.1$, $\tau = -0.04$). The solid line is the Theil-Sen slope and the thin, dotted line shows the bootstrapped 95% confidence intervals.



30

Figure 6. The event $\text{NO}_3^-_{\text{Atm}}$ yield (in g N ha^{-1}) has a 1:1 relationship with the estimated rainfall $\text{NO}_3^-_{\text{Atm}}$ deposition on impervious surfaces (in g N ha^{-1}) at GWN (slope = 1.00, intercept = 1, $r^2 = 0.55$, $p < 0.05$), but not at GUN.